Supplement of

Quantification of isomer-resolved iodide chemical ionization mass spectrometry sensitivity and uncertainty using a voltage-scanning approach

Chenyang Bi et al.

Correspondence to: Gabriel Isaacman-VanWertz (ivw@vt.edu)

Unit conversion from ions/mole/million reagent ions to cps/ppt/million reagent ions

We convert the sensitivity measured by the TAG-CIMS/FID to a direct-air-sampling CIMS operating at an assumed condition (2 slpm sampling flow rate; 2 slpm reagent ion flow rate; and 100 mbar ion-molecule reactor (IMR) pressure; and 293K ambient temperature) to help understand the data presented.

The typical unit for CIMS sensitivity, S^{typ}, is ions per second per million reagent ions per ppt, or cps/ppt/million reagent ions, which can be written as:

$$S^{typ} = \frac{i_X}{i_P} \times \frac{1}{t} \times \frac{n_{M,samp}}{10^{12} \, n_{X,samp}} \tag{1}$$

where i_X/i_P is the normalized ion count, i.e., number of ions from the analyte X ratioed to the number of ions of primary reagent ions (in millions), which is usually reported per unit time, t (typically 1 second). The term on the rate is the number of moles of sample flow, $n_{M,samp}$, per trillion moles X in the sample, $n_{X,samp}$, which is equivalent to ppt^{-1}. We can multiple both sides of the equation by volumetric flow rate of the sample, Q_{samp}, which can be written as a volume, V_{samp}, of flow being sampled per unit time (units of standard cm^3/s):

$$\frac{1}{Q_{samp}} S^{typ} = \frac{i_X}{i_P} \times \frac{1}{t} \times \frac{n_{M,samp}}{10^{12} \, n_{X,samp}} \times \frac{t}{V_{samp}} \tag{2}$$

This can be re-arranged and simplified as:

$$\frac{10^{12}}{Q_{samp}} S^{typ} = \frac{i_X}{i_P} \times \frac{1}{n_{X,samp}} \times \frac{n_{M,samp}}{V_{samp}} \tag{3}$$

The right-most term is the molar density of sample flow, which can be adjusted by Avogadro's number, A_V, to yield number density, $[M]_{samp}$, (units of molecules/cm^3):

$$\frac{10^{12}}{Q_{samp}} S^{typ} = \frac{i_X}{i_P} \times \frac{1}{n_{X,samp}} \times \frac{[M]_{samp}}{A_V} \tag{4}$$

Re-arranged, we see that:

$$\frac{10^{12} \, A_V}{Q_{samp}[M]_{samp}} S^{typ} = \frac{\frac{i_X}{i_P}}{n_{X,samp}} \tag{5}$$

The right-hand of this equation is normalized ions per moles, which is a unit of sensitivity conducive to GC analyses, S^{GC}. These two sensitivity units can thus be converted as:

$$S^{typ} = \frac{Q_{samp} \, [M]_{samp}}{10^{12} \, A_V} S^{GC} \tag{6}$$

Assuming a typical sample flow of approximately room temperature ambient air ($[M]_{samp}$ = 2.5×10^{19} molec/cm^3) and a sample flow, Q_{samp}, of 2 slpm (33.3 cm^3/s, standard), the conversion is $\frac{S^{typ}}{S^{GC}}$ = 1.4×10^{-15}. This is the conversion factor used to relate the left and right axis of Figure 3-5 though it is dependent on operating conditions.

Calculation of maximum sensitivity

The maximum kinetically limited sensitivity in units of cps/ppt/million reagent ions, S^{typ}_{kin}, was calculated using equation S1-3 described by Isaacman-Vanwertz et al., (2018), adjusted by a factor of 10^6 to provide units of per million reagent ions:

$$S^{typ}_{kin} = \frac{10^6 [M]_{IMR} f k_{coll} t_{IMR}}{10^{12}} \tag{7}$$

Where $[M]_{IMR}$ is the number density in the IMR, calculated as $[M]_{IMR}$ = 2.5×10^{18} molec/cm^3 at 100 mbar. The collisional rate, k_{coll}, between the analyte molecule and the reagent ion is assumed to be 1×10^{-9} cm^3 molec^{-1} s^{-1}.

Sensitivity is dependent in part on the fraction, f, of total flow in the IMR consisting of sample, calculated as:

$$f = \frac{Q^0_{samp}}{Q^0_{samp} + Q^0_{reag}} \tag{8}$$

the ratio of sample flow rate to the total flow rate (i.e., sample + reagent flows) entering the IMR, where ^{0} superscript denotes that both flows are referenced to a standard temperature and pressure. Under these conditions (Q^0_{samp} 0.7 sccm and Q^0_{reag} = 2000 sccm), f = 3.50×10^{-4}.

Collisions occur throughout the residence time in the IMR, t_{IMR}, which can be calculated as the time the total volumetric flow takes to sweep the physical volume of the IMR, V_{IMR}, at the adjusted from standard pressure (P^0) to the operating pressure of the IMR, P_{IMR}:

$$t_{IMR} = \frac{V_{IMR}}{(Q^0_{samp} + Q^0_{reag}) \frac{P^0}{P_{IMR}}} \tag{9}$$

Because ratios of pressure are proportional to ratios of number density, this equation can be re-written in terms of standard and IMR number density:

$$t_{IMR} = \frac{V_{IMR}}{(Q^0_{samp} + Q^0_{reag}) \frac{[M]^0}{[M]_{IMR}}} \tag{10}$$

The residence time of molecules in the IMR, t_{IMR}, is calculated as 0.14 s based on a pressure of 100 mbar and a volume of 47 cm^3.

The kinetically limited maximum sensitivity can be calculated in units of ions per mole per million reagent ions by combining Eqs. 6 and 7:

$$S_{kin}^{GC} = \frac{10^6 [M]_{IMR} f k_{coll} t_{IMR} A_V}{Q_{samp} [M]_{samp}} \tag{11}$$

Both Q_{samp} and $[M]_{samp}$ are proportional to temperature and pressure, so the denominator of this equation is equivalent to moles/time, $\frac{V_{samp}}{t} \times \frac{n_{M,samp}}{V_{samp}} = \frac{n_{M,samp}}{t}$ (i.e., mass flow rate). This is useful, as it implies that the kinetic sensitivity is independent of the pressure and temperature of the GC effluent, which varies throughout the GC run. For use in this equation, both terms can consequently be adjusted to standard temperature and pressure, Q_{samp}^0 and $[M]^0$:

$$S_{kin}^{GC} = \frac{10^6 [M]_{IMR} f k_{coll} t_{IMR} A_V}{Q_{samp}^0 [M]^0} \tag{12}$$

Substituting Eqs. 8 and 10 into 12, a complete description of kinetically limited maximum sensitivity in GC-conducive units can be obtained:

$$S_{kin}^{GC} = \frac{10^6 ([M]_{IMR})^2 k_{coll} V_{IMR} A_V}{([M]^0)^2 \left(Q_{samp}^0 + Q_{reag}^0\right)^2} \tag{13}$$

Using the same proportionality between pressure and number density, this can be simplified as:

$$S_{kin}^{GC} = 10^6 k_{coll} V_{IMR} A_V \left(\frac{P_{IMR}}{P^0}\right)^2 \left(Q_{samp}^0 + Q_{reag}^0\right)^{-2} \tag{14}$$

Under GC-CIMS operation, $Q_{samp}^0 = 0.7$ sccm (0.012 cm³/s), $Q_{reag}^0 = 2000$ sccm (33.3 cm³/s), and $P_{IMR} = 100$ mbar, so $S_{kin}^{GC} = 2.5 \times 10^{17}$ ions/mole/million reagent ions. Using the same instrument design, Isaacman-Vanwertz et al., (2018) found the experimentally observed maximum sensitivity to be a factor of 4 lower than calculated kinetically-limited sensitivity, so we estimate that the maximum sensitivity is within the range from 6.4×10^{16} to 2.5×10^{17} ions/mole/million reagent ions.

These values translate into S_{kin}^{typ}= 90 to 350 cps/ppt/million reagent ions using unit conversion described in Eq. 6. However, we note that is higher than actual kinetically-limited sensitivity calculated under typical ambient operating conditions, (Q_{samp}^0= 2000 sccm) because in the GC-CIMS, there is more time for reaction in the IMR due to lower sample flows (Q_{samp}^0= 0.7 sccm). Under typical ambient operating conditions at the IMR pressure used, Q_{samp}^0= 2000 sccm should be used instead in Eq. 14. After unit conversion using Eq. 6, S_{kin}^{typ} = 88 cps/ppt/million reagent ions (Eq. 7).
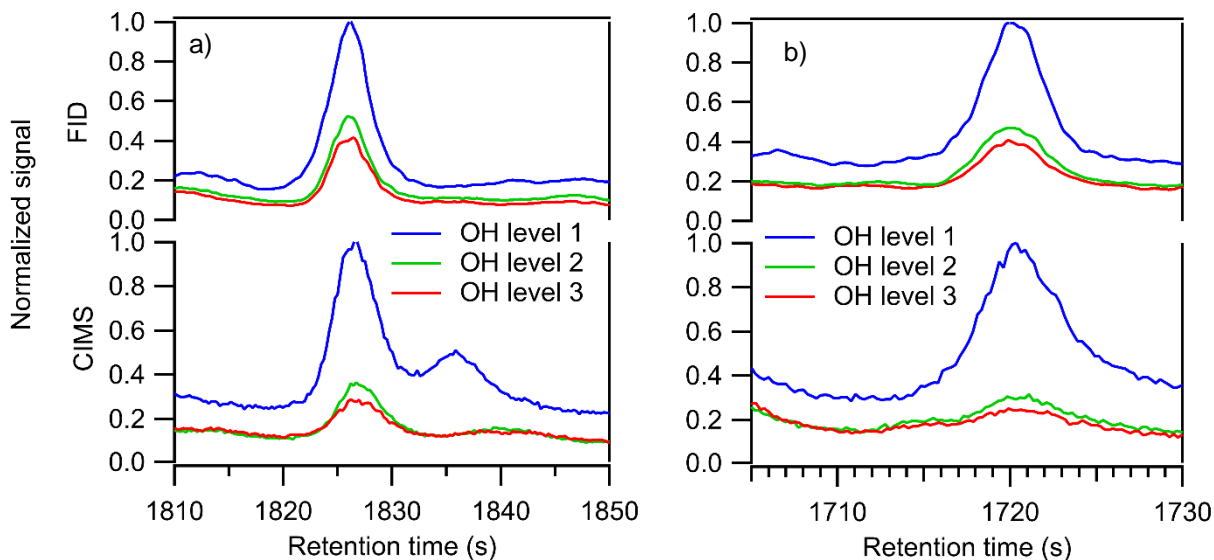
Figure S1. Comparison of CIMS and FID peaks at different OH exposure levels for a) Compound 4 and b) Compound 3.

Calculation of dV₅₀ of a mixture of isomers

When a formula has a mixture of multiple isomers with varying signals, the true dV_{50} of the formula should be obtained using the sigmoid fit of the summed signal fraction remaining versus dV. However, to simplify the calculation of formula-based dV_{50}, this study applied signal-weighted average of dV_{50} of each isomers to obtain the dV_{50} of a formula. Here, we demonstrate this signal-weighted dV_{50} is a good approximation of the true dV_{50} using simulated data.
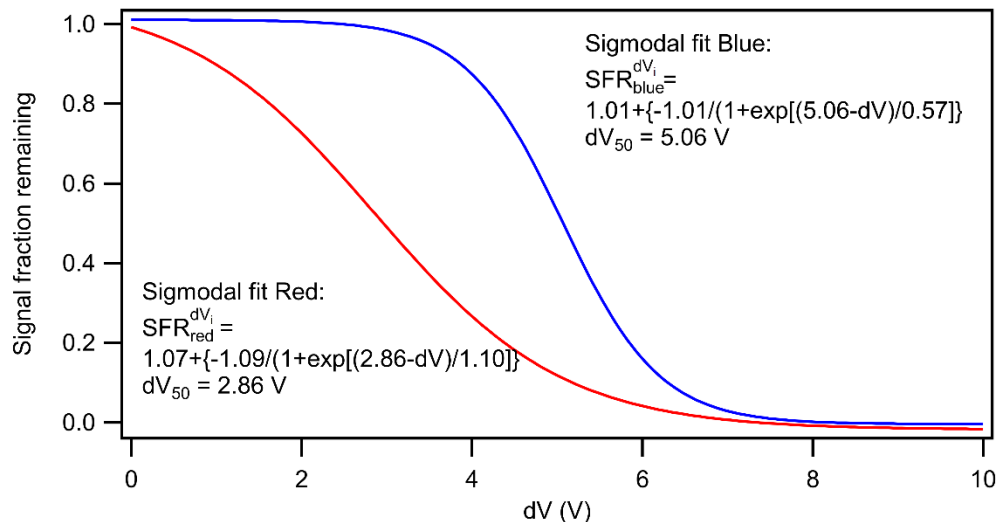
Figure S2. Simulated sigmoid fits of two isomers.

In Figure S2, we examine simulated sigmoid voltage scanning curves of two isomers within a formula ("red" and "blue") described by representative randomly selected coefficients. The signal fraction remaining ($SFR_{formula}^{dV_i}$) of the formula (i.e., the sum of the two isomers) at a given voltage setting (dV_i would described by the signal weighted average of the two curves:

$$SFR_{formula}^{dV_i} = \frac{S_{red}^{base}\left(SFR_{red}^{dV_i}\right)+S_{blue}^{base}\left(SFR_{blue}^{dV_i}\right)}{\left(S_{red}^{base}+S_{blue}^{base}\right)} \tag{15}$$

Where S_{red}^{base} and S_{blue}^{base} are signal of the two isomers at baseline voltages; $SFR_X^{dV_i}$ is the signal fraction remaining of each isomer at a given voltage setting.

Using Eq. 15, the expected sigmoidal curve can be obtained describing signal fraction remaining of the combined isomers for a given ratio of isomers. In other words, a signal fraction remaining curve can be generated for the formula by summing the two isomers at their given ratio . Rather than solving for dV_{50} analytically (which may get complex for multiple isomers), the combined curve can be fit with a sigmoidal function to calculate the "true dV_{50}" that would be observed for the formula. This can be compared to the "signal-weighted dV_{50}" calculated as the signal-weighted average of the dV50 of the two isomers. Numerical solutions for two isomers are presented here to determine the accuracy of using a simplified signal-weighted dV_{50} approach, across two orders of magnitude of relative ratio.
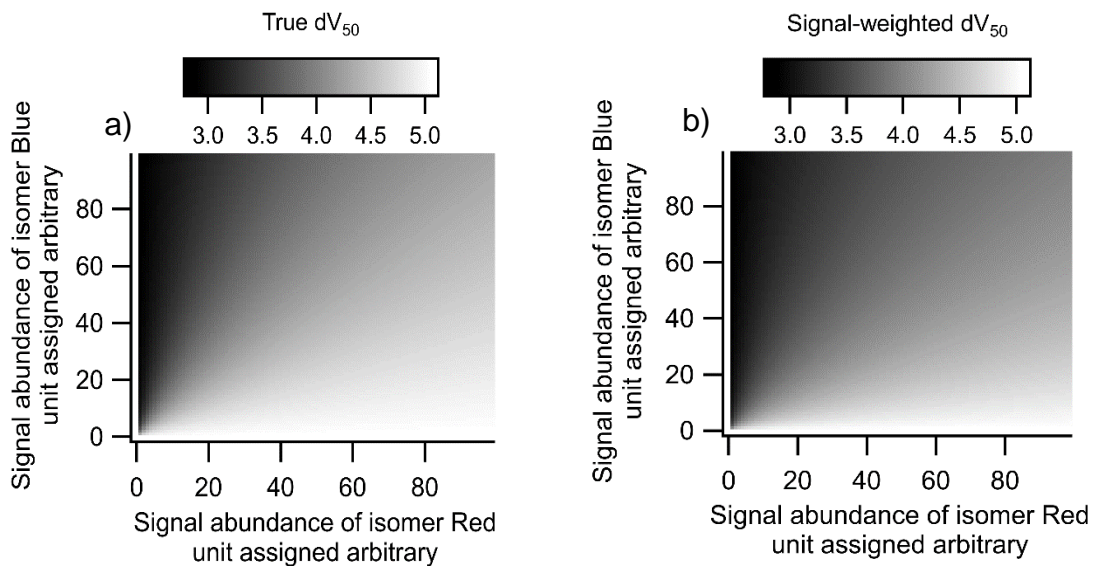
Figure S3. The distribution of a) true dV_{50} and b) signal-weighted dV_{50} of the formula with varying isomer abundance.
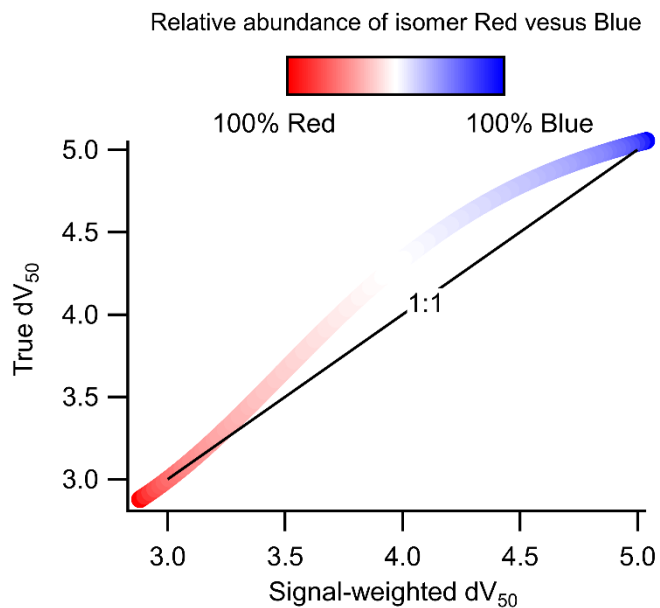
Figure S4. Comparison of true dV_{50} and signal-weighted dV_{50}. The curve colored with red shows signals dominated by isomer Red while the blue section suggest that signals are dominated by isomer Blue. Color scale is logarithmic.

An arbitrary signal from 0-100 is assigned each to the "red" and "blue" isomers, implying two orders of magnitude differences in signals of the two isomers at baseline voltage. From Figure S3 it is clear that the signal-weighted dV_{50} is

similar to the true dV_{50} (calculated from sigmoid fit of Eq 15) under the two orders of magnitude variance in isomer abundance. The difference between true and signal-weighted dV_{50} (i.e. Figure S3a vs. S3b) is shown in Figure S4 as a function of the relative ratio of the isomers. When the signals of the two isomers are roughly equal (white region in the colored curved), the deviation reaches the maximum, but is still well within 10% and an absolute value of <0.5 V. On average, the deviation is only a few percent. This deviation is lower than the threshold of maximum relative standard deviation of dV_{50} in duplicated samples, and is generally within the uncertainty of most fits, so is unlikely to contribute substantial uncertainty.
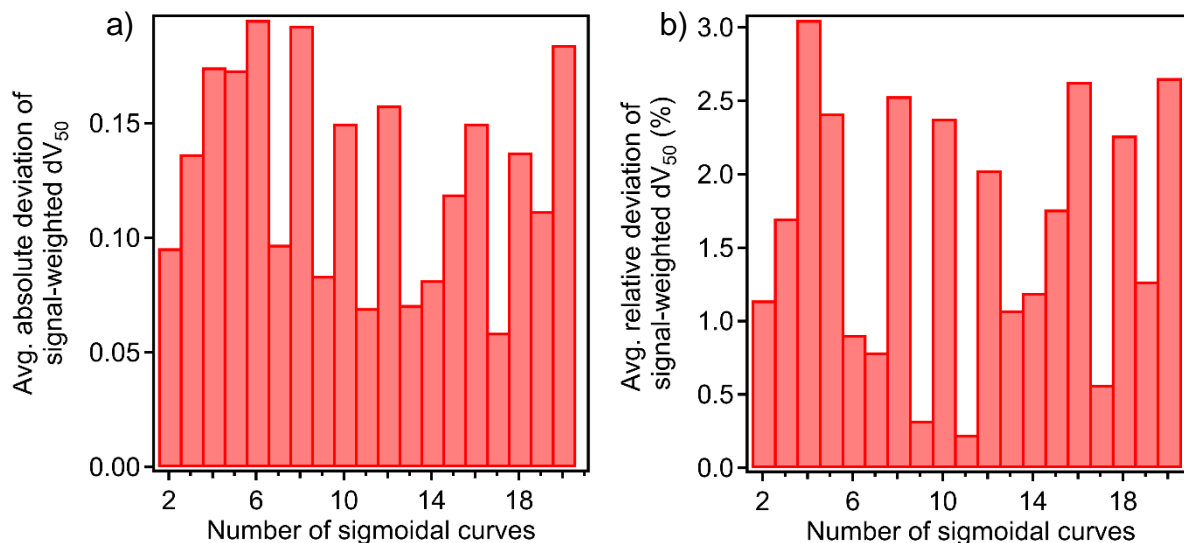
Figure S5. The average (a) absolute and (b) relative deviation of the true true dV_{50} from the signal-weighted dV_{50} for formulas with 2-20 isomers.

We generalize this result by numerically expanding to formulas with more than two isomers, generating a set of a given number of sigmoidal curve, each with randomly-assigned dV_{50}, sigmoidal rate coefficients, and relative signal between 3 – 9, 0.2 - 1, and 1 - 100, respectively. A Monte-Carlo analysis of 1000 such sets was conducted for each number of curves to examine the average absolute and relative deviation of the true dV_{50} from the signal-weighted dV_{50}. The results suggest that the average absolute deviations are within 0.2 V and the average relative deviations are within 3% between the true and signal-weighted dV_{50}. No clear trend is observed in error with the increase in the number of curves, though the significant noise in the data may obscure any such trend. Therefore, we can conclude that the signal-weighted approach to calculate dV_{50} of a formula is a good approximation of the true dV_{50}.

Table S1. The elemental formula and sensitivity of compounds presented in Figure 3. Note that only formulas containing 2 or more isomers with calculated sensitivity are included.

Oxidation experiment	Elemental formula	Isomer No.	Mean sensitivity (ions/mole/million reagent ions)
Limonene-O_3	C7H10O3	1	1.77E+16
		2	4.83E+14
	C8H12O3	1	1.34E+16
		2	1.64E+14
	C9H10O2	1	3.72E+14

		2	1.38E+16
	C9H12O4	1	4.37E+15
		2	8.20E+15
		3	2.43E+15
		4	6.58E+15
		5	1.26E+16
		6	8.36E+16
	C9H14O3	1	1.26E+16
		2	7.86E+16
		3	1.34E+16
		4	7.18E+15
		5	1.37E+17
	C9H16O3	1	1.32E+16
		2	1.33E+16
	C10H14O3	1	1.23E+16
		2	2.94E+16
		3	1.79E+16
	C10H16O4	1	9.11E+16
		2	1.16E+17
		3	2.27E+16
Limonene-OH	C5H6O4	1	1.09E+15
		2	2.20E+14
		3	8.70E+14
	C7H10O3	1	2.54E+16
		2	1.21E+16
	C7H10O4	1	4.03E+16
		2	2.48E+16
	C8H10O4	1	2.67E+16
		2	5.44E+16
	C8H8O4	1	4.91E+14
		2	5.83E+15
	C9H12O4	1	5.04E+15
		2	3.05E+16
		3	4.13E+16
		4	4.90E+15
		5	1.54E+16
	C9H14O3	1	6.37E+15
		2	9.28E+15

		3	4.75E+15
	C9H14O4	1	3.09E+16
		2	2.56E+16
		3	1.30E+16
		4	6.46E+14
		5	1.52E+15
	C10H14O3	1	4.83E+15
		2	8.15E+15
	C10H16O4	1	8.13E+16
		2	2.52E+16
		3	6.63E+16
		4	1.75E+16
TMB-OH	C8H10O4	1	1.33E+15
		2	6.03E+16
	C8H12O4	1	9.67E+15
		2	3.55E+16
	C9H12O4	1	1.84E+15
		2	8.78E+15
		3	6.58E+16
	C9H12O5	1	3.16E+15
		2	1.15E+16
	C9H14O4	1	6.83E+16
		2	7.40E+16
	C9H14O5	1	1.38E+16
		2	1.06E+16
		3	4.40E+15
		4	2.00E+15
		5	1.38E+15

Table S2. The elemental formula, sensitivity, and dV_{50} of compounds presented in Figure 4. Note that only compounds with both calculated sensitivity and dV_{50} are included.

Oxidation experiment	Compound No.	Elemental formula	Sensitivity (ions/mole/million reagent ions)		dV_{50} (V)	
			Mean	Standard deviation	Mean	Standard deviation
Limonene-O_3	1	C5H6O4	6.10E+14	8.67E+13	6.21	0.33
	2	C7H10O2	1.23E+15	2.67E+14	5.49	0.23

3	C7H10O3	4.83E+14	1.16E+14	5.09	0.29
4	C7H8O4	1.46E+15	1.24E+14	6.44	0.35
5	C8H12O3	1.34E+16	4.52E+14	5.86	0.48
6	C8H12O3	1.64E+14	5.06E+13	5.37	0.25
7	C8H12O4	3.95E+16	7.77E+15	6.14	0.21
8	C9H10O2	3.72E+14	1.49E+14	5.19	0.30
9	C9H10O2	1.38E+16	1.83E+14	4.64	0.74
10	C9H12O4	4.37E+15	9.09E+14	4.93	0.36
11	C9H12O4	8.20E+15	4.30E+14	5.98	0.37
12	C9H12O4	2.43E+15	2.38E+14	4.71	0.74
13	C9H12O4	6.58E+15	1.98E+15	5.62	0.35
14	C9H12O4	1.26E+16	1.17E+15	4.53	0.47
15	C9H12O4	8.36E+16	3.14E+16	6.62	0.44
16	C9H14O3	1.26E+16	3.78E+15	4.87	0.60
17	C9H14O3	7.86E+16	5.34E+15	6.25	0.33
18	C9H14O3	1.34E+16	1.49E+15	5.19	0.48
19	C9H14O3	7.18E+15	1.50E+14	4.49	0.84
20	C9H14O4	5.77E+16	3.57E+15	6.39	0.62
21	C9H16O3	1.32E+16	2.58E+14	5.43	0.26
22	C9H16O3	1.33E+16	1.25E+15	5.20	0.74
23	C10H14O3	1.23E+16	9.40E+14	5.08	0.73
24	C10H14O3	2.94E+16	2.78E+15	5.81	0.32
25	C10H14O3	1.79E+16	1.51E+15	5.66	0.42
26	C10H16O4	9.11E+16	1.09E+16	6.96	0.26
27	C10H16O4	1.16E+17	2.67E+16	7.51	0.22
28	C10H16O4	2.27E+16	5.54E+15	5.97	0.32
Limonene-OH	1	C5H6O4	1.09E+15	1.01E+14	4.97	0.41
	2	C5H6O4	8.7E+14	4.30E+14	3.61	0.18
	3	C7H10O3	2.54E+16	1.24E+16	4.74	0.52
	4	C7H10O3	1.21E+16	8.53E+14	5.64	0.24
	5	C7H10O4	4.03E+16	4.31E+15	5.57	0.24
	6	C7H10O4	2.48E+16	4.69E+15	5.64	0.22
	7	C8H10O4	2.67E+16	3.69E+15	4.41	0.41
	8	C8H8O4	5.83E+15	1.15E+15	3.72	0.61
	9	C9H12O4	5.04E+15	9.40E+14	5.27	0.25
	10	C9H12O4	3.05E+16	5.46E+15	5.34	0.33
	11	C9H12O4	4.13E+16	8.40E+15	5.66	0.53
	12	C9H14O3	6.37E+15	1.99E+13	5.35	0.94

	13	C9H14O4	3.09E+16	3.65E+15	5.38	0.23
	14	C9H14O4	2.56E+16	8.96E+15	5.73	0.43
	15	C9H14O4	1.3E+16	1.25E+15	4.89	0.46
	16	C9H14O4	1.52E+15	2.21E+14	5.44	0.86
	17	C10H16O4	8.13E+16	9.26E+15	6.56	0.24
	18	C10H16O4	2.52E+16	3.99E+15	5.06	0.35
	19	C10H16O4	6.63E+16	6.88E+15	6.39	0.43
	20	C10H16O4	1.75E+16	1.28E+15	5.35	0.50
	1	C8H10O4	1.33E+15	1.23E+14	3.59	0.67
	2	C8H10O4	6.03E+16	2.05E+15	5.72	0.47
	3	C8H12O4	9.67E+15	3.38E+15	4.11	0.60
	4	C8H12O4	3.55E+16	5.41E+15	4.35	0.58
	5	C9H12O4	1.84E+15	9.02E+14	4.84	0.20
	6	C9H12O4	8.78E+15	8.04E+14	4.55	0.45
	7	C9H12O4	6.58E+16	3.11E+16	5.41	0.37
TMB-OH	8	C9H12O5	3.16E+15	1.37E+15	6.51	0.38
	9	C9H12O5	1.15E+16	5.16E+15	5.54	0.22
	10	C9H14O4	6.83E+16	2.98E+16	5.38	0.46
	11	C9H14O4	7.40E+16	3.06E+16	6.73	0.24
	12	C9H14O5	1.38E+16	3.50E+15	6.73	0.31
	13	C9H14O5	1.06E+16	4.87E+15	6.31	0.25
	14	C9H14O5	4.40E+15	1.09E+15	5.67	0.44
	15	C9H14O5	1.38E+15	2.25E+14	5.52	0.99

References

Isaacman-Vanwertz, G., Massoli, P., O'Brien, R., Lim, C., Franklin, J. P., Moss, J. A., Hunter, J. F., Nowak, J. B., Canagaratna, M. R., Misztal, P. K., Arata, C., Roscioli, J. R., Herndon, S. T., Onasch, T. B., Lambe, A. T., Jayne, J. T., Su, L., Knopf, D. A., Goldstein, A. H., Worsnop, D. R. and Kroll, J. H.: Chemical evolution of atmospheric organic carbon over multiple generations of oxidation, Nat. Chem., 10(4), 462–468, doi:10.1038/s41557-018-0002-2, 2018.